# Adhesion of Individual Attachment Setae of the Spider *Cupiennius salei* to Substrates With Different Roughness and Surface Energy

*Bastian Poerschke, Stanislav N. Gorb and Clemens F. Schaber\**

*Functional Morphology and Biomechanics, Zoological Institute, Kiel University, Kiel, Germany*

Dynamic adhesion is a key ability for animals to climb smooth surfaces. Spiders evolved, convergent to geckos, a dry adhesive system made of setae branching into smaller microtrichia ending as spatulae. Several previous studies concentrated either on the whole adhesive claw tuft on the spider´s foot that consists of attachment setae or on the single adhesive contact elements, the microtrichia with spatula-shaped tips. Here, the adhesion of single setae of the spider *Cupiennius salei* was examined and the morphology of the pretarsus and the fine structure of the setae were studied in further detail. Using individual setae fixed to force sensing cantilevers, their adhesion at different contact angles with a glass substrate was measured as well as their adhesive performance on substrates with different roughness and on smooth surfaces with different surface energies. The results show an individual variability of the adhesive forces corresponding to the seta morphology and especially to the seta tip shape. The tip shapes of the setae vary largely even in neighboring setae of the pretarsal claw tuft that comprises approximately 2,400 setae. Regarding surface energy of the substrate, the adhesion force on hydrophobic polytetrafluoroethylene was 30% of that on a hydrophilic glass substrate, which points to the importance of both van der Waals interactions and hydrogen bonds in spider adhesion.

Keywords: adhesion, claw tuft, locomotion, pretarsus, scopula, spider hair, surface properties

## INTRODUCTION

The ability to climb almost every surface is a big advantage for animals. Therefore, many species convergently evolved different types of adhesive footpads to perform locomotion even on smooth vertical surfaces. One of these types is a soft bubble based smooth adhesive system that has been discovered for example in *Orthoptera, Hymenoptera, Solifugae and Scincidae*. The second type are fibrillary/hairy, seta based adhesive pads found for example in *Dipterans, Coleopterans, Araneae, Gekkonidae and Anolinae* (Gorb and Heepe, 2017). Among the animal groups using fibrillary pads, the geckos (*Gekkonidae*) and spiders (*Araneae*) developed an exceptionally effective reversible adhesive system for so called "dry adhesion" that works without any sticky fluid involved. In geckos, the dry adhesive system consists of a multitude of keratinous setae that branch at the tips and are arranged in lamella on the toes (Rizzo et al., 2006). In spiders, the dry adhesive system for locomotion is located on the most distal leg parts (pretarsi) and made up of chitinous setae bundled in the so-called scopula claw tuft. From each of these setae, a multitude of microtrichia branch off, which are

arranged densely close to the seta tips and face the substrate (Niederegger and Gorb, 2006; Schaber et al., 2019). As in geckos, the terminal contact elements of the setae are flat and thin platelet-shaped spatulae.

Adhesion of the dry attachment systems is enhanced by shearing, which promotes alignment of the spatulae with the substrate surface and increases the contact area for attractive van der Waals forces (Wolff and Gorb, 2013; Flenner et al., 2020). In the gecko, the adhesive force of a single seta strongly depended on its sliding in contact with a substrate. The adhesion force ranged from 0.6 µN without sliding, to 13.6 µN with sliding, and 194 µN at 5 µm sliding and a preload of 15 µN. Assuming that all setae were simultaneously and maximally attached, these data indicated an adhesive force of 100 N of the single gecko foot (Autumn et al., 2000). In the jumping spider *Evarcha arcuata*, the adhesive force of a single spatula was measured to be 38 nN. The assumption that all spatulae were in contact resulted in an adhesive force that could support 173 times the body weight of the animal (Kesel et al., 2003; Kesel et al., 2004). In the Central American wandering spider species *Cupiennius salei*, which was also used in the present study, the adhesion of a single leg scopula on glass when shear force was applied was found to be 35 mN, which would suffice to hold an adult female animal on a vertical surface. However, the vertical pull-off force without shear preload was zero (Wohlfart et al., 2014). The arrangement of the spatulae on the setae was previously explained to be most important for the spider's traction forces on different micro-rough substrates in the species *Philodromus dispar* (Wolff and Gorb, 2012a).

Up to now, the adhesive forces of the single spider setae that make up the adhesive scopula on the claw tufts of the spider remained unknown. To find out more on the interplay of the adhesive setae with different kinds of substrates, here we examined the morphology of the claw tuft and the setae and measured adhesion forces of individual setae on various characterized substrates with different surface energies and roughness and at different setal contact angles on glass.

## MATERIALS AND METHODS

### Animal Sample Preparation
Air-dried exuviae of the last molt of female wandering spiders of the species *Cupiennius salei* (Barth, 2002) were used for reflected light microscopy and scanning electron microscopy. Individual setae were plucked in the center of the pretarsal scopulae from autotomized legs of adult female specimen that were bred and raised in the Department of Functional Morphology and Biomechanics at Kiel University and kept at temperatures between 20 and 25°C and relative humidity of 70–100%. For *in vivo* examination of adhesion, spiders were anesthetized and fixed upside-down to a sample holder using adhesive tape.

### Surface Samples
Different rough surfaces with the same surface chemistry were fabricated in a two-step casting technique. First, casts were taken from glass slides, polishing papers with different defined roughness (P0.05, P1, P3, P9, and P12; Buehler Ltd., Lake

Bluff, IL, United States) and sand papers (P800, P1500, P2500; Bauhaus GmbH, Mannheim Germany) using polyvinyl siloxane (Coltène President light body; Coltène Whaledent AG, Altstätten, Switzerland). In the second step, these negative impressions were cast using epoxy resin (low viscosity kit; Electron Microscopy Sciences, Hatfield, PA, United States). The smooth surfaces for testing adhesion at different surface energies were uncoated glass slides, silicon wafers, polytetrafluoroethylene (PTFE; Goodfellow Ltd. Huntingdon, United Kingdom), and epoxy resin casts of glass slides.

### Microscopy
Reflected light microscopy was performed using a Leica M205A microscope equipped with a Leica DFC420 camera (Leica Microsystems GmbH, Wetzlar, Germany) in multifocus imaging mode. For scanning electron microscopy, single setae were fixed to the sample holders using conductive carbon adhesive tape. Whole pretarsi were additionally mounted using conductive carbon cement (LEIT-C; Plano GmbH, Wetzlar, Germany). The samples were examined without sputter coating using a Hitachi S-4800 (Hitachi Ltd., Tokyo, Japan) scanning electron microscope at an acceleration voltage of 3 kV or sputter coated with 10 nm gold-palladium using a Hitachi TM3000 at 15 kV. Plucked single setae were inspected in 70% ethanol cover slipped on glass slides using a transmitted light microscope (Axioplan; Carl Zeiss Microscopy GmbH, Jena, Germany) equipped with a digital camera (AxioCam MRc).

### Surface Characterization
The surface energy and its polar and disperse shares were characterized on the four different smooth substrates using a contact angle measurement system (OCA20; DataPhysics Instruments, Filderstadt, Germany). The contact angle of three different liquids (double distilled water, diiodomethane, ethylene glycol) was measured on ten random spots of each substrate. The polar and disperse shares of the surface energy were calculated using the software of the instrument, and the mean values determined for each substrate.

For roughness characterization, 3D surface measurements were performed using a white light interferometer (NewView 6k; Zygo Corporation, Middlefield, Connecticut, United States). Using the software MetroPro (version 8.1.5) of the instrument, height maps were plotted and their surface roughness determined in µm as the root mean square deviation of the roughness profile (*rms* roughness).

### Adhesion Force Measurements
Piezo-electric force sensing cantilevers (FMT-120b; Kleindiek Nanotechnik, Reutlingen, Germany) mounted on a micromanipulator (MM3A; Kleindiek Nanotechnik, Reutlingen, Germany) were calibrated by pushing the tip against a calibrated spring. Calibration curves were plotted from the cantilever deflection measured using white light interferometry and recordings of the corresponding voltage signal from the force measurement amplifier (FMS-01; Kleindiek Nanotechnik, Reutlingen, Germany). The sensitivities of the cantilevers were in the range between
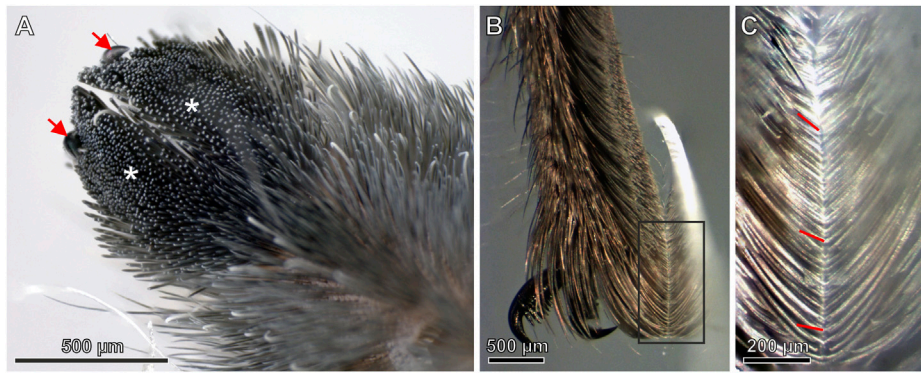
**FIGURE 1 | (A)** Ventral surface of the two-lobed pretarsal scopula claw tuft (blackish; asterisks) comprising the tips of thousands of densely arranged setae. Arrows mark the claws **(B)** Side view of the pretarsal scopula in contact with a glass slide **(C)** Magnified view of the rectangle marked in **(B)**. There is a notable increase of the angles of the seta tips with the glass surface from top (proximal) toward the bottom (distal) of the image caused by the increased curvature of the setae. Exemplarily, the lines indicate the angles of individual seta tips with the substrate.

2.7 μN V$^{-1}$ and 6.5 μN V$^{-1}$ (linear regression coefficients $R^2 \geq$ 0.995).

The adhesion force measurements were performed under a reflected light microscope (LMS310; Carl Zeiss Microscopy GmbH, Jena, Germany) equipped with a digital camera (BLS 5 MP; BMS microscopes b.v., Capelle aan den IJssel, Netherlands). The cantilevers with single setae glued to their tips using polyvinyl siloxane as well as the substrates were arranged in side view. For the tests, the cantilevers were pushed vertically onto the substrate up to a force of 0.5 μN using the software NanoControl 3.1 (Kleindiek Nanotechnik, Reutlingen, Germany) and immediately pulled off. The sampling rate of the analogue/digital converter was set to 10 kHz and the data smoothened by a moving average calculation of 100 data points. The adhesion peaks just before the loss of contact between the setae and the substrates were used for further analysis. All measurements were performed at temperatures between 22.8°C and 26.1°C and at relative humidity between 31 and 58.7%. For statistical analysis the software SigmaPlot (12.5; Systat Software, Inc. San Jose, CA, United States) and R Studio (R Studio Inc. Boston, United States) were used.

## RESULTS
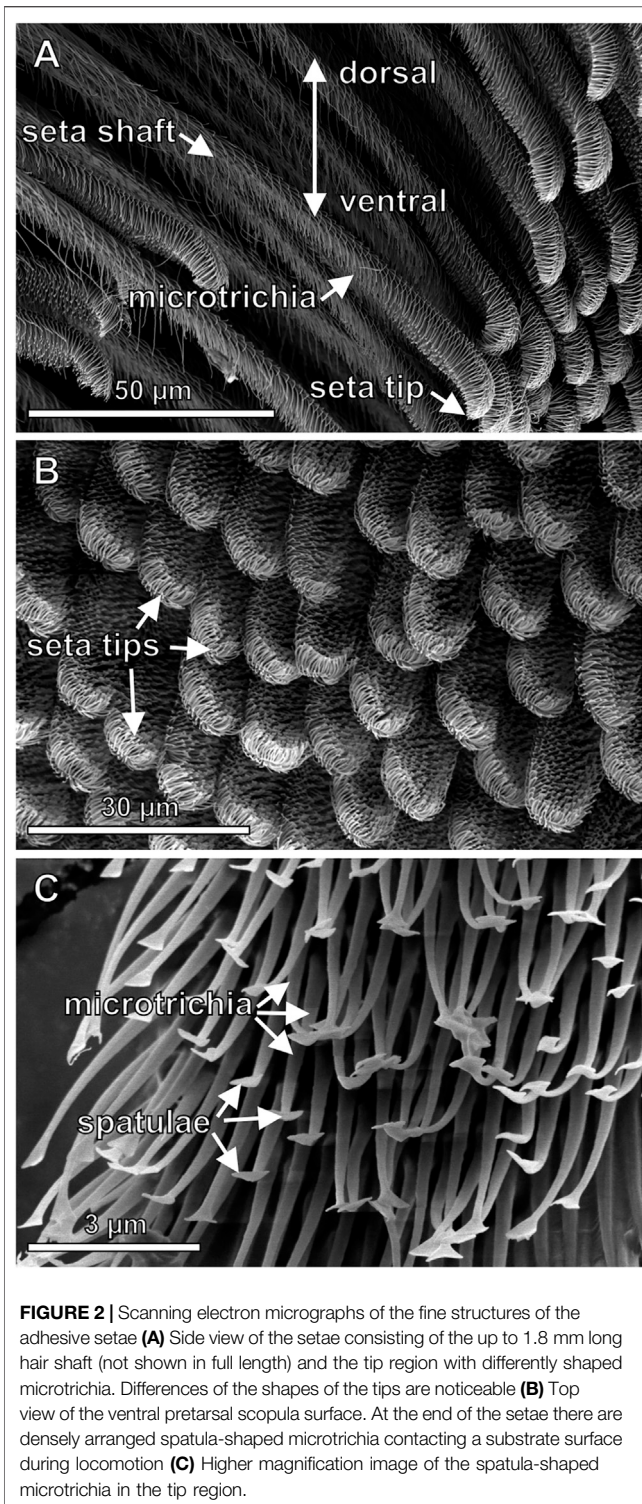
### Morphology of the Pretarsus

Besides the adhesive setae of the scopula, on the pretarsus there are two claws for clamping on compliant and rough substrates. Additionally, in between of the claws there is a much shorter middle hook. The ventral side of the pretarsus is two-lobed and densely covered by the adhesive setae (**Figure 1A**). The seta tips of the pad form a rather flat sole-like surface that well gains contact with a substrate surface (**Figure 1B**). The setae show an increased curvature in their distal parts so that the angles at which their tips approach a substrate increase from approximately 45° in the proximal part of the scopula up to approximately 90° in the most distal part (**Figure 1C**).

### Morphology of the Adhesive Setae

Using SEM on partly shaved pretarsi showed highly ordered regular arrangement of the setae of the scopulae. The single setae are densely covered with branching microtrichia. In the uppermost 30 μm of the seta, its shape appears flatter and the density of microtrichia increases, especially on the ventral side facing the substrate upon contact (**Figure 2A**). The distance between the seta tips amounts to 10–15 μm (**Figure 2B**). On the ventral side, the microtrichia of the tip regions consist of less than 1 μm thick narrowing stalks with flattened ends, the spatulae, that are responsible for building up contact with the substrate and generating adhesion force (**Figure 2C**). No spatulae were found on the dorsal sides of the setae. In the SEM, after some exposure to the electron beam, the previously separated spatulae attracted each other and congregated.

### Seta Adhesion at Different Contact Angles

The individual setae used for the force measurements were plucked from the mid-region of the scopula. The three randomly selected setae clearly showed different curvatures and tip shapes (**Figures 3A–C**). For the determination of a significant angle for the measurements of adhesion on different substrates, the adhesion forces of the individual setae were measured at different contact angles with smooth glass (**Figures 3D–F**, **4**). Seta 1 showed increasing adhesion with decreasing contact angles. With 412 ± 15 nN (mean ± standard deviation; $n$ = 12 measurements), adhesion was highest at an angle of 38°. However, because of the curvature of the seta, this angle could only be reached at the edge of the glass substrate. Therefore, the naturally more realistic angle of 45° was used for the further measurements. The measurements of adhesion for seta 2 showed a peak force of 277 ± 13 nN at approximately 61°, a smaller peak of 187 ± 16 nN at 72°, and constantly high values between 232 ± 10 nN and 319 ± 7 nN in the range from 83° to 97°. Here, the angle of 85° close to the force maximum was selected for the further measurements. The adhesion values of seta 3 did not vary as much as those of setae 1 and 2 and they were in the range between 120 ± 11 nN and

**FIGURE 2 |** Scanning electron micrographs of the fine structures of the adhesive setae **(A)** Side view of the setae consisting of the up to 1.8 mm long hair shaft (not shown in full length) and the tip region with differently shaped microtrichia. Differences of the shapes of the tips are noticeable **(B)** Top view of the ventral pretarsal scopula surface. At the end of the setae there are densely arranged spatula-shaped microtrichia contacting a substrate surface during locomotion **(C)** Higher magnification image of the spatula-shaped microtrichia in the tip region.

179 ± 6 nN at angles from 49° to 80°. The lowest adhesive force of 99 ± 8 nN was measured at an angle of 85°. At higher angles, adhesion increased again, and 88° was chosen for the measurements on different substrates (**Figure 4**).

## Seta Adhesion to Surfaces With Different Surface Energies
### Substrate Surface Properties
The *rms* roughness values for the four smooth substrates were 0.006 ± 0.002 μm for the glass, 0.131 ± 0.011 μm for the epoxy resin mold of the glass surface, 0.002 ± 0.001 μm for the silicon, and 0.014 ± 0.001 μm for the PTFE surface (mean values ± standard deviations of measurements on five different areas of the substrates).

The contact angles of water on the different smooth substrates indicated the strongest hydrophilicity for the glass surface with a contact angle of 31.9 ± 11.6° (mean ± standard deviation; $n = 10$). The epoxy resin and silicon surfaces were slightly hydrophilic with contact angles of 85.2 ± 1.6°, and 84.9 ± 4.6°, respectively. The PTFE surface showed hydrophobic properties with a contact angle of water of 103.9 ± 3.8°.

The surface energies calculated from the contact angles of the different liquids showed the highest value for the hydrophilic glass surface with a total of 59.24 J m$^{-2}$ dominated by a polar share of 44.13 J m$^{-2}$ (74.5%), and a disperse share of 15.11 J m$^{-2}$ (25.5%). The total values of the surface energy and the distribution of its shares were similar for the epoxy resin and the silicon surface. The values for the epoxy resin were 30.33 J m$^{-2}$ dominated by a disperse share of 25.26 J m$^{-2}$ (83.3%), and a polar share of 5.07 J m$^{-2}$ (16.7%). The surface energy of the silicon surface was 28.45 J m$^{-2}$ with a disperse share of 22.70 J m$^{-2}$ (79.8%) and a polar share of 5.75 J m$^{-2}$ (20.2%). The lowest value of surface energy was found for the hydrophobic PTFE with 18.07 J m$^{-2}$ as the sum of 16.61 J m$^{-2}$ (91.9%) disperse and 1.46 J m$^{-2}$ (8.1%) polar shares (**Figure 5A**).

### Adhesion Forces on Smooth Substrates With Different Surface Energies
The highest adhesive force of the setae was measured on the glass with 263 ± 86 nN (mean ± standard deviation; $N = 3$ setae, $n = 108$ measurements) and a median value of 262 nN. The mean adhesion force on the epoxy resin surface was 156 ± 56 nN and a median of 142 nN; that to the silicon amounted to 174 ± 61 nN and a median of 188 nN. The weakest adhesion was found on the PTFE substrate with 82 ± 53 nN (median 81 nN). A box plot of the results is shown in **Figure 5B**. Kruskal-Wallis one way analysis of variance (ANOVA) on ranks indicated very high statistically significant difference ($p < 0.001$) of the adhesion values between the substrates. An all pairwise multiple comparison procedure (Tukey test) of the data on a significance level of $p < 0.05$ yielded significant differences between all the surfaces except for silicon and the epoxy resin. **Figures 5C,D** clearly show increasing seta adhesion with increasing polarity of the substrates and no or little influence of the disperse shares. Correlation statistics for the influence of relative humidity using the Spearman method gained a not significant $p$ value of 0.0992 for all measurements, which were performed in a humidity range between 31 and 58.7%.

## Seta Adhesion on Substrates With Different Roughness
### Morphology and Roughness of the Test Substrates
The surface P0 (glass mold) was smooth. The white light interferometric height maps showed increasing grain sizes,
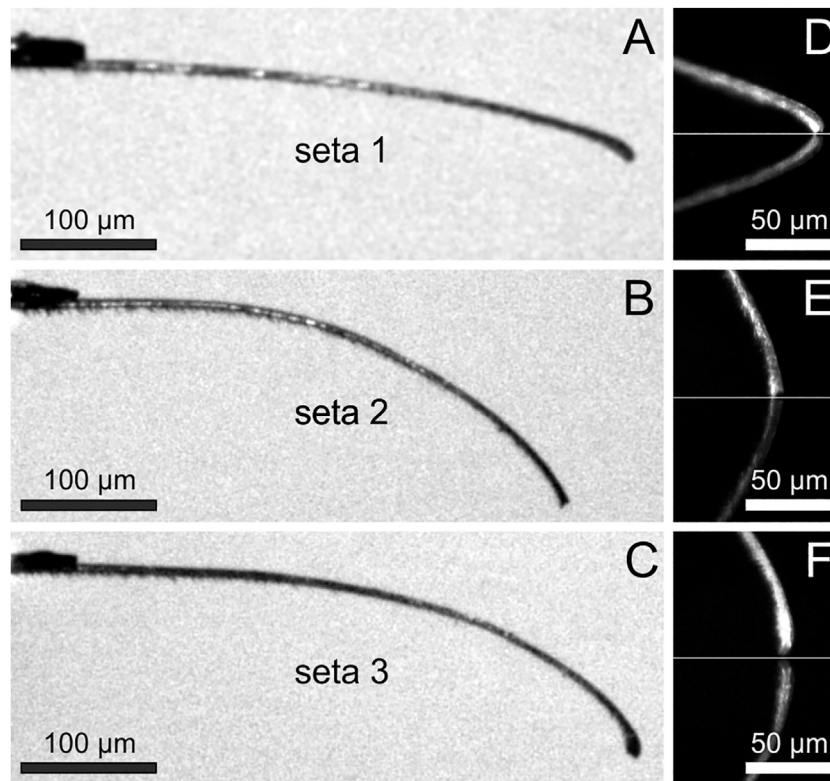
**FIGURE 3 | (A–C)** Individual adhesive setae in side view fixed to the force sensing cantilevers (top left). Note the different curvatures and tip shapes of the setae taken randomly from the center of the pretarsal scopula **(D–F)** Tip regions of the setae shown in **(A–C)** adhering to a glass surface (marked by the white horizontal lines) at the angles used for the measurements on different substrates. Below the white lines, the mirror images of the setae are visible. The angles of the most distal 20 µm of the setae with the glass surface were measured to be 44.8° for seta 1, 85.1° for seta 2, and 88.4° for seta 3.
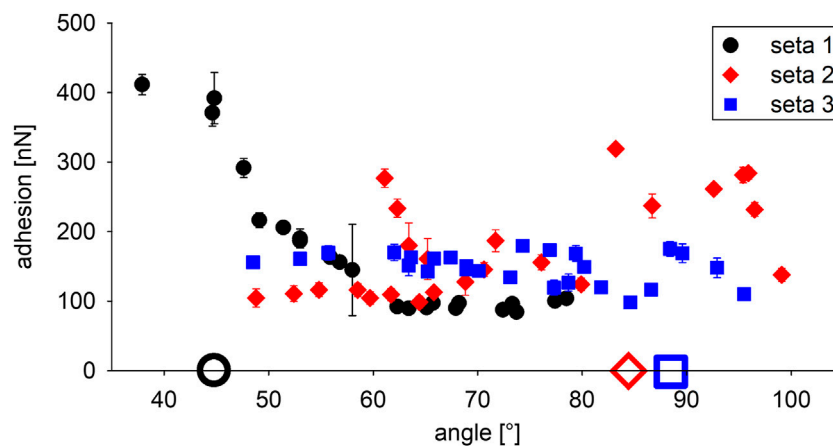


**FIGURE 4 |** Adhesion of the three different attachment setae at different angles with the glass substrate. The full symbols show mean values ± standard deviation of 12 measurements each. The large open symbols on the *x*-axis indicate the angles of the individual setae shown in **Figures 3D–F** chosen for the further measurements on different substrates.

height differences, and irregularities of the surface structures from P0.05 to P12 (molds of polishing papers). Small granules were visible in the molds of the polishing papers P3, P9, and P12 in addition to the larger asperity structures. The shapes of the grains of the sand paper molds SP1 and SP2 were more distinct. In SP2 the grains were larger compared to those in SP1 and
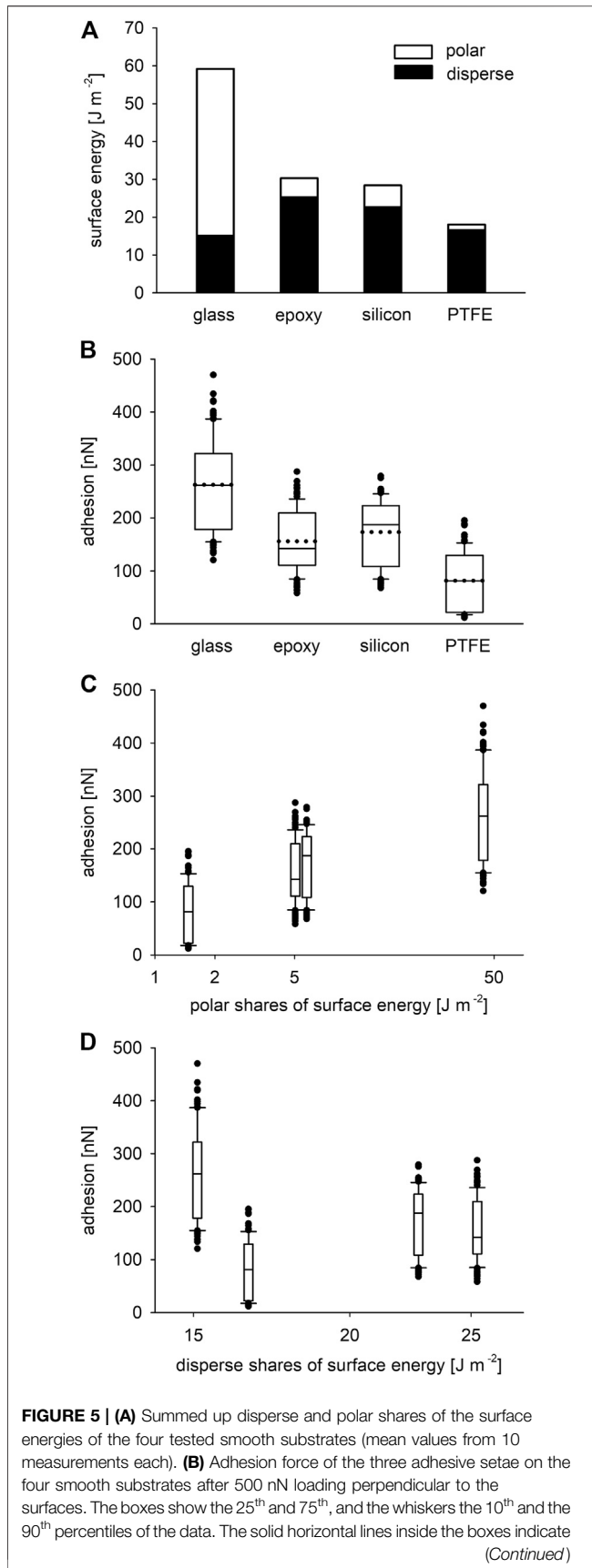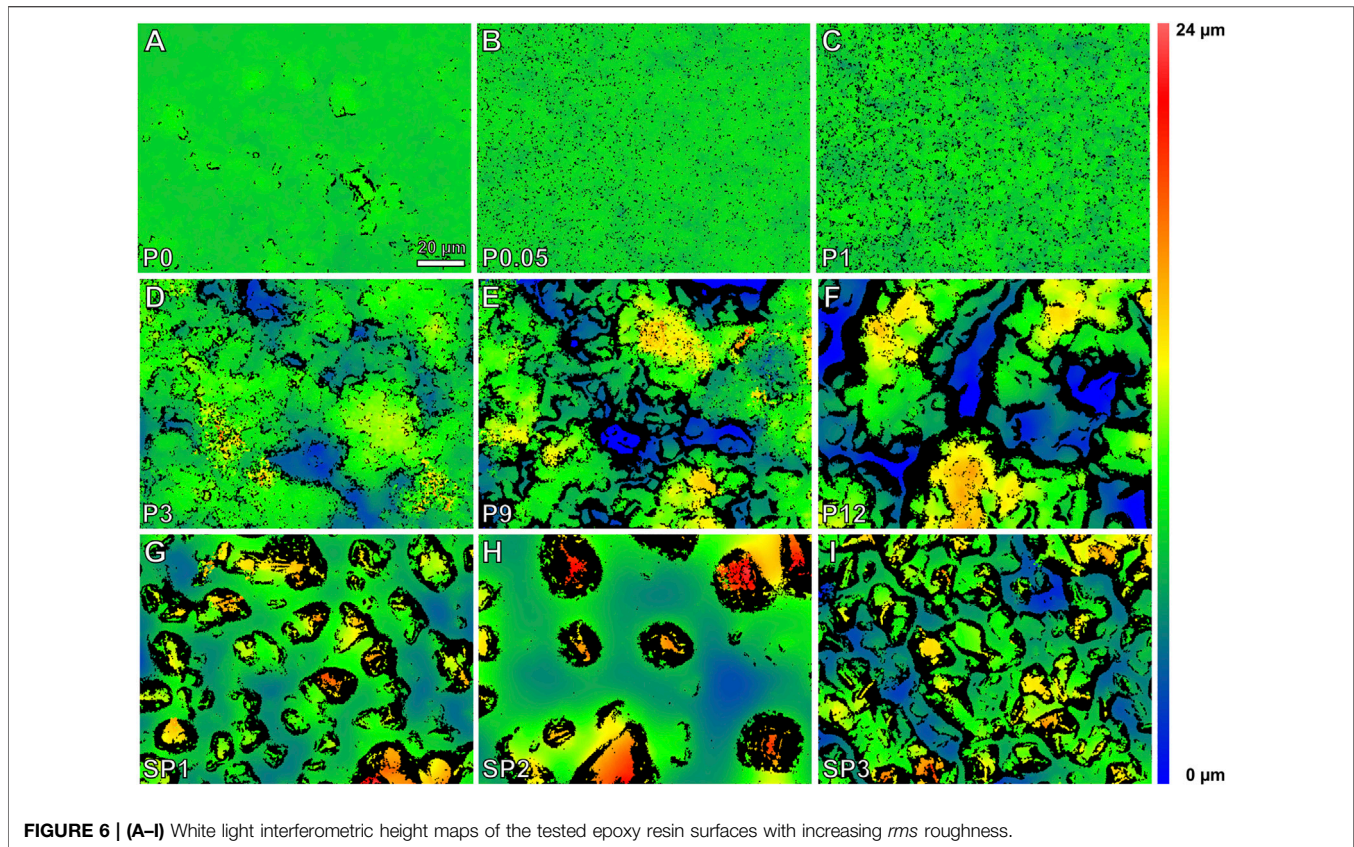
highest in comparison to all other samples. The sand paper mold SP3 showed the highest degree of irregularity having smaller but more densely arranged grains of different shapes (**Figure 6**). The mean *rms* roughness values of these nine different rough substrate surfaces are plotted in **Figure 7A**.

## Adhesion Forces on Different Rough Substrates

Adhesive forces of individual setae considerably differed on all tested surfaces and no general trend is indicated by the data (**Figure 7B**). For seta 1, the mean values of adhesion force were the highest on all substrates except for P3. For seta 1, there was a trend toward stronger adhesion to surfaces with increasing *rms* roughness up to $533 \pm 249$ nN ($n = 36$) on substrate SP3. In addition, the standard deviations increased with increasing mean values of adhesion force. Adhesion values obtained for seta 2 were generally lower ($<200$ nN) than those of seta 1. Seta 2 did not show any trend of adhesion force on the differently rough substrates, with mean values between $67 \pm 31$ nN on substrate P12 and $160 \pm 48$ nN on substrate P3. Adhesion forces of seta 3 were the lowest on all substrates with the minimum values of $34 \pm 13$ nN on the relatively smooth substrate P1 and $34 \pm 16$ nN on the rough SP2. The maximum value of $100 \pm 24$ nN was measured on the smooth substrate P0. Without considering the individual setae, a statistical comparison of all pooled values using a pairwise *t*-test and a Tukey HSD test indicated that the adhesion force on the substrates P0.05 and SP2 was significantly lower than on all other substrates and significantly higher on SP3.

## DISCUSSION

The examination of the general morphology of the pretarsus of *Cupiennius salei* in the present study showed the claws and the two lobed claw tufts of scopula setae. This finding confirms those of previous authors (Wolff and Gorb, 2013; Labarque et al., 2017). It enables the spider to use the specific attachment mechanism dependent on the geometry and the mechanical properties of the substrate. The claws are assumed to enable clamping on soft or very rough surfaces, whereas the adhesive setae are used for adhesion to smoother and hard surfaces (**Figures 1B,C**). The setae themselves are covered with differently shaped microtrichia. The microtrichia with pointed tips along the shaft can be interpreted as spacers similar to those of other spider species (Eggs et al., 2015) and avoid that the setae to stick to each other. The increased density of the spatula-shaped microtrichia in the tip region and their arrangement toward the substrate make them well suited to make contact with a surface during locomotion. This hierarchical structure of the pretarsal attachment system of spiders is different from the structure of fibrillary adhesive systems of insects, e.g. in

**FIGURE 5 | (A)** Summed up disperse and polar shares of the surface energies of the four tested smooth substrates (mean values from 10 measurements each). **(B)** Adhesion force of the three adhesive setae on the four smooth substrates after 500 nN loading perpendicular to the surfaces. The boxes show the 25th and 75th, and the whiskers the 10th and 90th percentiles of the data. The solid horizontal lines inside the boxes indicate
*(Continued)*

FIGURE 6 | (A–I) White light interferometric height maps of the tested epoxy resin surfaces with increasing *rms* roughness.
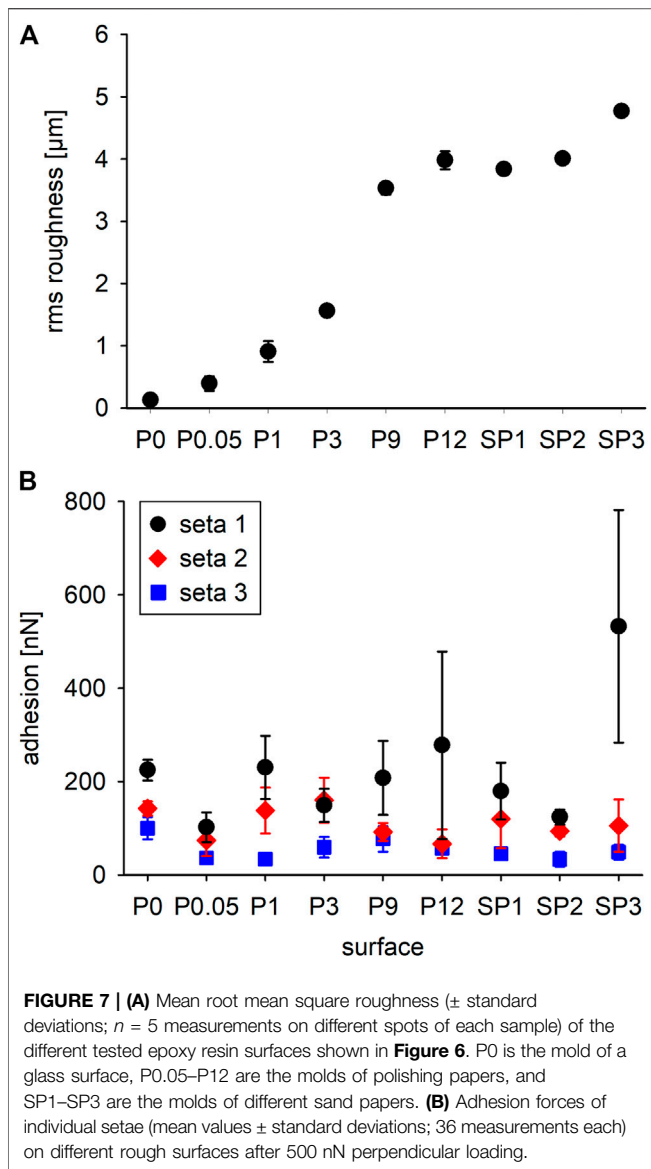
beetles and earwigs, which are made up of shorter, unbranched setae on the tarsi (Haas and Gorb, 2004; Gilet et al., 2018).

On the smooth substrates with different surface energy, the setae adhered best to the glass, which also exhibited the highest hydrophilicity and a highest amount the polar shares of surface energy (**Figure 5**). For adhesion, the polar shares are responsible for hydrogen bonds between two materials. The disperse shares result in attractive van der Waals forces (Autumn et al., 2002). On the epoxy resin and the silicon surface that are only slightly hydrophilic and for which the amount of disperse shares of surface energy are similarly high, the adhesive force of the setae dropped down to approximately two thirds of that on glass. On the hydrophobic and non-polarizable PTFE substrate, the adhesive forces of the setae was lowest and approximately 30% of those on glass.

For the gecko seta, it has been shown that its adhesion purely relies on van der Waals forces, because the adhesive forces were the same on polarizable hydrophilic and hydrophobic substrates and confirmed the model prediction (Autumn et al., 2002). For a single Gecko spatula, however, adhesion increased with increasing relative air humidity and substrates with increasing hydrophilicity (Huber et al., 2005), and the authors suggested monolayers of water being adsorbed between the spatulae and the substrate leading to additional capillary forces. For the spider setae, here we show stronger adhesion on the hydrophilic glass surface with a high polar share of surface energy, which makes the

influence of thin layers of water on the adhesion strength likely. For different spider species with scopulae, the capillary forces between the thin water layer on a substrate and the scopula hairs were found to be most important for their adhesion (Homann, 1957). On the polarizable epoxy resin and the silicon substrate, which mainly exhibit disperse shares of surface energy, the adhesion of the spider setae is still fair. Together with the presence of adhesive force on the hydrophobic non-polarizable PTFE substrate, these findings lead to the conclusion that a combination of van der Waals forces and hydrogen bonds between polar substrates and the spatulae is responsible for the adhesion of the attachment setae of *Cupiennius salei* on substrates with different surface energies. Capillary forces may also play an important role especially at higher relative humidity, because it has been shown that the shear adhesion of the spider *Philodromus dispar* on an epoxy resin substrate was highest at a relative humidity of 60% (Wolff and Gorb 2012b).

The tests for seta adhesion on differently rough surfaces were performed on the same material of epoxy resin molds to avoid different chemistry of the substrates. The small adhesion forces of the setae to the P0.05 substrate likely result from its *rms* roughness of 396 nm and the size of the spatulae. This roughness may be too small for the single spatulae to form proper contact. For the reduced adhesion to the SP2 surface, the interplay between the substrate morphology and the seta size likely is the limiting factor. The grains on the SP2 substrate appear

**FIGURE 7 | (A)** Mean root mean square roughness (± standard deviations; $n$ = 5 measurements on different spots of each sample) of the different tested epoxy resin surfaces shown in **Figure 6**. P0 is the mold of a glass surface, P0.05–P12 are the molds of polishing papers, and SP1–SP3 are the molds of different sand papers. **(B)** Adhesion forces of individual setae (mean values ± standard deviations; 36 measurements each) on different rough surfaces after 500 nN perpendicular loading.

spherically shaped and spread on a rather flat surface. For an approaching seta, it is crucial whether it hits a grain and which aspect of the seta tip – the one with or the one without the spatula – gets in contact on top or at the edges of the grain. If the seta tip makes contact with its spatula-free side at the edges of the grains, adhesion forces will be low. It can be assumed that the surface morphology of the SP2 substrate strongly inhibits proper contact making of the spatulae. The statistically significantly increased adhesion value of the setae on the roughest substrate SP3 results from the high adhesion force of the seta 1. Both seta 2 and seta 3 on SP3 do not show values higher than on other substrates. The obvious different adhesion of different setae to the substrates with different roughness indicates that most likely the tip shape and the distribution of the spatulae plays the key role for the attachment of the individual setae. Neighboring setae plucked from the center of the claw tuft scopula showed four different tip

shapes and arrangements of the tip microtrichia in four randomly selected setae (**Figure 8A**).

Shear force applied on an already attached seta, however not sliding the seta, was shown to largely increase the pull-off force from 3.6 µN up to 25 µN by the alignment of a large number of spatulae with a smooth glass surface (Flenner et al., 2020). In the present study, no shear force was applied on the three individual tested setae. Therefore, we measured the result of the arrangement of the spatulae, which spontaneously aligned with the substrate structures upon contact. For such an adhesive behavior, the tip shapes and the arrangement of the microtrichia and spatulae of the seta is crucial for the adhesive force generation. The tip shapes of the three individual tested setae clearly differed (**Figures 8B–D**), as most likely did the arrangement of the spatulae. As can be seen in **Figure 4**, adhesion on glass greatly differed at different contact angles of the setae. The mostly higher adhesion forces of seta 1 at the angle of 45° may be the result of the orientation of the spatula-rich side of the seta toward the structural features of the rough substrates. The higher number of the flexible microtrichia and spatulae are more likely to find proper surface features to attach. For seta 2 and seta 3, the angles of 85°, and 88°, respectively, were also selected within ranges of high adhesion for the respective setae. However, their adhesion on differently rough surfaces was low compared to that of seta 1. For seta 2, at the chosen angle of 85°, likely only the microtrichia next to the tip contacted the substrate with their sides. This lead to alignment and adhesion of a smaller number of spatulae and less adhesive force compared to seta 1. Seta 3 showed the lowest adhesion on the differently rough epoxy resin surfaces. Considering the angle of 88° chosen for the measurements and the rounded shape of the tip, it appears likely that seta 3 contacted the surface with the backbone and not with the ventral side, rich in spatula-shaped microtrichia, which resulted in reduced attachment forces.

Even when taking the highest adhesive value of 830 nN into account and assuming that all 18,800 setae (~2,350 per leg; Wolff and Gorb, 2012c) of the spider were in contact with a substrate, the resulting adhesive force of approximately 16 mN could not support the body weight (~3.6 g) of an adult female spider. Since *Cupiennius salei* easily climbs vertical surfaces and is able to walk upside-down also on smooth surfaces, there must be mechanisms of adhesion other than those examined in the single setae in the present study. Interestingly, the adhesive setae are not rigidly fixed in the pretarsal cuticle. In the natural situation, the movability of the setae toward the substrate is strictly limited by a stopper-like structure of the basal hair shaft directly at the insertion of the seta in its socket (**Figure 9**). This stopper keeps the position of the seta fixed in its position in the socket at dorsad movements of the claw tuft to facilitate pulling-off. On the dorsal (distal) side of the socket, however, there is some space that allows a seta deflection by approximately 6–7° when placed onto a substrate. In our experiments, the setae were well fixed to the stiff silicon cantilevers. In the natural situation, the flexibility of the seta suspension in the pretarsal cuticle may help each individual seta of the claw tuft to find better contact with the structural features of the substrate and consequently a good place to adhere. This movability of the setae also supports their
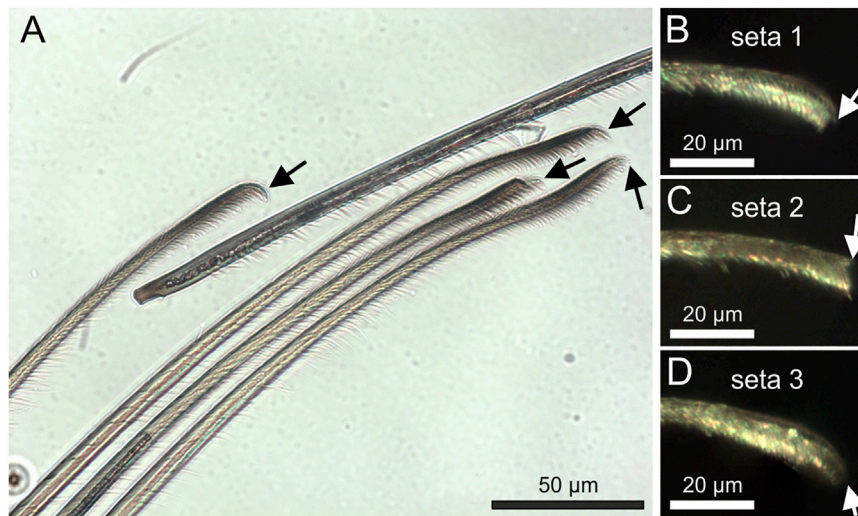
**FIGURE 8 | (A)** Transmitted light microscopic side view of a bunch of neighboring attachment setae plucked from the center of the pretarsal scopula. Different tip shapes (arrows) are clearly visible **(B–D)** Reflected light microscopic images of the tips of the setae used for the adhesion measurements in the experimental setup. The arrows point to the tips of the seta backbone.
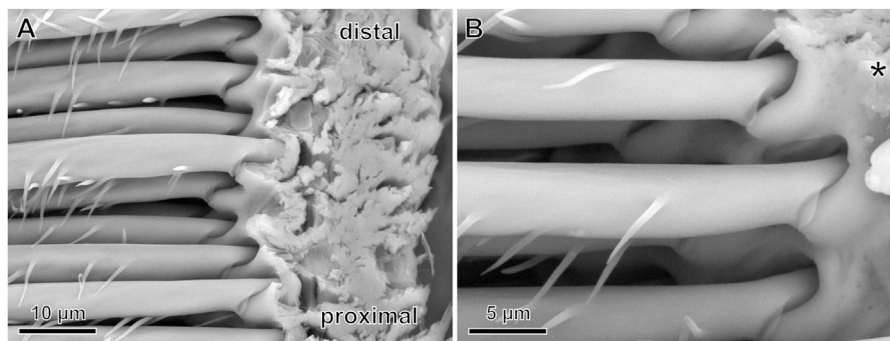


**FIGURE 9 |** SEM images of the bases of pretarsal adhesive setae and their insertion into the cuticle in a vertically dissected exuvia cuticle. **(A)** On the left are the most proximal parts of the adhesive setae. At their insertion in the cuticle, the hair shaft is narrowed and a stopper-like structure is situated on the ventral (lower) aspect. Distal and proximal refer to the arrangement the claw and the leg. **(B)** Magnified cuticle insertion region of the setae. The asterisk exemplary marks the pivot point of a seta for dorsad (upward) deflections.

shearing in order to bring more adhesive spatulae in contact with the substrate (see Flenner et al., 2020), which likely resulted in the better adhesion of *Cupiennius*, when opposing leg pairs were in contact with the ground at pulling-off the whole spider (Wohlfart et al., 2014). Considering the previously measured 25 µN adhesive force of a single attachment seta preloaded in shear, 1,400 setae in contact (which is less than two thirds of the setae of a single leg) would suffice for an adult female *Cupiennius salei* to adhere on smooth glass. Interestingly, adhesion of the whole scopula claw tuft was zero at vertical pulling-off even after shearing (Wolff and Gorb, 2013; Wohlfart et al., 2014). In the present study the single setae did show adhesive forces at vertical pulling-off on all the different substrates tested. These results indicate that the specific movements of the individual setae of the claw tuft may be most important for making adhesive contact with the substrate.

The results of the present study indicate a distribution of different adhesive tip shapes of the adhesive setae, which likely represents an adaptation of the spider attachment system for efficient interaction with substrates of different roughness. The cuticle of *Cupiennius salei* has been reported to have an effective Young's modulus of 18 GPa (Blickhan and Barth, 1985). For the individual seta, the specific structural arrangement of the mechanically stiffer dorsal seta backbone (Schaber et al., 2019) and the softer ventral "brush" of spatula-shaped microtrichia is crucial for adhesion at certain angles with the substrate. It can be assumed that the individual morphology of each individual seta and its position within the scopula orchestration are optimized for maximal adhesion on natural substrates with many different properties as found in the habitat of the spider.

The individual variability of the morphology of the spider attachment setae, which is strongly interdigitated with their adhesive performance, has been shown here for the first time. Furthermore, we reveal the importance of examining the relevant different length and force scales for understanding the functionality of specific structures in the entire adhesive system of the spider. This knowledge can lead to new bioinspired materials with outstanding properties such as nanostructured reversible residue-free dry adhesives e.g. based on cellulose nanofibers (Schaber et al., 2018), carbon nanotubes (Bhushan et al., 2008; Schaber et al., 2015a; Schaber et al., 2015b; Su et al., 2020; Yang et al., 2020) or other polymeric materials (Xue et al., 2012; Pattantyus-Abraham et al., 2013; Xue et al., 2013; Borodich and Savencu 2017; Di Tan et al., 2020).

## DATA AVAILABILITY STATEMENT

The raw data supporting the conclusions of this article will be made available by the authors, without undue reservation.

## REFERENCES

Autumn, K., Liang, Y. A., Hsieh, S. T., Zesch, W., Chan, W. P., Kenny, T. W., et al. (2000). Adhesive Force of a Single Gecko Foot-Hair. *Nature* 405, 681–685. doi:10.1038/35015073

Autumn, K., Sitti, M., Liang, Y. A., Peattie, A. M., Hansen, W. R., Sponberg, S., et al. (2002). Evidence for van der Waals adhesion in gecko setae. *Proc. Natl. Acad. Sci.* 99, 12252–12256. doi:10.1073/pnas.192252799

Barth, F. G. (2002). *A Spider´s World: Senses and Behavior*. Berlin: Springer. doi:10.1007/978-3-662-04899-3

Bhushan, B., Galasso, B., Bignardi, C., Nguyen, C. V., Dai, L., and Qu, L. (2008). Adhesion, Friction and Wear on the Nanoscale of MWNT Tips and SWNT and MWNT Arrays. *Nanotechnol.* 19, 125702. doi:10.1088/0957-4484/19/12/125702

Blickhan, R., and Barth, F. G. (1985). Strains in the Exoskeleton of Spiders. *J. Comp. Physiol.* 157, 115–147. doi:10.1007/bf00611101

Borodich, F. M., and Savencu, O. (2017). "Hierarchical Models of Engineering Rough Surfaces and Bio-Inspired Adhesives," in *Bio-inspired Structured Adhesives, 179–219.* Editors L. Heepe and L. Xue (Basel: Springer International).

Eggs, B., Wolff, J. O., Kuhn-Nentwig, L., Gorb, S. N., and Nentwig, W. (2015). Hunting without a Web: How Lycosoid Spiders Subdue Their Prey. *Ethol.* 121, 1166–1177. doi:10.1111/eth.12432

Flenner, S., Schaber, C. F., Krasnov, I., Stieglitz, H., Rosenthal, M., Burghammer, M., et al. (2020). Multiple Mechanical Gradients Are Responsible for the strong Adhesion of Spider Attachment Hair. *Adv. Mater.* 32, 2002758. doi:10.1002/adma.202002758

Gilet, T., Heepe, L., Lambert, P., Compère, P., and Gorb, S. N. (2018). Liquid Secretion and Setal Compliance: the Beetle's Winning Combination for a Robust and Reversible Adhesion. *Curr. Opin. Insect Sci.* 30, 19–25. doi:10.1016/j.cois.2018.08.002

Gorb, S. N., and Heepe, L. (2017). "Biological Fibrillar Adhesives: Functional Principles and Biomimetic Applications," in *Handbook of Adhesion Technology.* Editors L. da Silva, A. Öchsner, and R. Adams (Cham: Springer).

Haas, F., and Gorb, S. (2004). Evolution of Locomotory Attachment Pads in the Dermaptera (Insecta). *Arthropod Struct. Dev.* 33, 45–66. doi:10.1016/j.asd.2003.11.003

Homann, H. (1957). Haften Spinnen an einer Wasserhaut? *Naturwissenschaften* 44, 318–319. doi:10.1007/bf00630926

Huber, G., Mantz, H., Spolenak, R., Mecke, K., Jacobs, K., Gorb, S. N., et al. (2005). Evidence for Capillarity Contributions to Gecko Adhesion from Single Spatula Nanomechanical Measurements. *Proc. Natl. Acad. Sci.* 102, 16293–16296. doi:10.1073/pnas.0506328102

Kesel, A. B., Martin, A., and Seidl, T. (2003). Adhesion Measurements on the Attachment Devices of the Jumping Spider *Evarcha Arcuata*. *J. Exp. Biol.* 206, 2733–2738. doi:10.1242/jeb.00478

Kesel, A. B., Martin, A., and Seidl, T. (2004). Getting a Grip on Spider Attachment: an AFM Approach to Microstructure Adhesion in Arthropods. *Smart Mater. Struct.* 13, 512–518. doi:10.1088/0964-1726/13/3/009

Labarque, F. M., Wolff, J. O., Michalik, P., Grisworld, C. E., and Ramírez, M. J. (2017). The Evolution and Function of Spider Feet (Araneae: Arachnida): Multiple Acquisitions of Distal Articulations. *Zool J. Linn. Soc-lond*, 181, 308–341. doi:10.1093/zoolinnean/zlw030

Niederegger, S., and Gorb, S. N. (2006). Friction and Adhesion in the Tarsal and Metatarsal Scopulae of Spiders. *J. Comp. Physiol. A.* 192, 1223–1232. doi:10.1007/s00359-006-0157-y

Pattantyus-Abraham, A., Krahn, J., and Menon, C. (2013). Recent Advances in Nanostructured Dry Adhesives. *Front. Bioeng. Biotechnol.* 1, 22. doi:10.3389/fbioe.2013.00022

Rizzo, N. W., Gardner, K. H., Walls, D. J., Keiper-Hrynko, N. M., Ganzke, T. S., and Hallahan, D. L. (2006). Characterization of the Structure and Composition of Gecko Adhesive Setae. *J. R. Soc. Interf.* 3, 441–451. doi:10.1098/rsif.2005.0097

Schaber, C. F., Filippov, A. E., Heinlein, T., Schneider, J. J., and Gorb, S. N. (2015b). Modelling Clustering of Vertically Aligned Carbon Nanotube Arrays. *Interf. Focus.* 5, 20150026. doi:10.1098/rsfs.2015.0026

Schaber, C. F., Flenner, S., Glisovic, A., Krasnov, I., Rosenthal, M., Stieglitz, H., et al. (2019). Hierarchical Architecture of Spider Attachment Setae Reconstructed from Scanning Nanofocus X-ray Diffraction Data. *J. R. Soc. Interf.* 16, 20180692. doi:10.1098/rsif.2018.0692

Schaber, C. F., Heinlein, T., Keeley, G., Schneider, J. J., and Gorb, S. N. (2015a). Tribological Properties of Vertically Aligned Carbon Nanotube Arrays. *Carbon* 94, 396–404. doi:10.1016/j.carbon.2015.07.007

Schaber, C. F., Kreitschitz, A., and Gorb, S. N. (2018). Friction-active Surfaces Based on Free-Standing Anchored Cellulose Nanofibrils. *ACS Appl. Mater. Inter.* 10, 37566–37574. doi:10.1021/acsami.8b05972

Su, Y. L., Hou, X. Y., Jiang, S. Y., Li, M., Liu, Y. M., Yang, Z., et al. (2020). Adhesion Properties of Carbon Nanotube Arrays for an Adhesive Foot of a Space Crawling Robot. *Smart Mater. Struct.* 29, 025001. doi:10.1088/1361-665x/ab5ad4

Tan, D., Luo, A., Wang, X., Shi, Z., Lei, Y., Steinhart, M., et al. (2020). Humidity-modulated Core-Shell Nanopillars for Enhancement of Gecko-Inspired Adhesion. *ACS Appl. Nano Mater.* 3, 3596–3603. doi:10.1021/acsanm.0c00314

## AUTHOR CONTRIBUTIONS

CS and SG conceived of the research. CS and BP designed the experiments. BP conducted the experiments and analyzed the data. BP, CS, and SG interpreted the data. BP wrote the first draft. CS edited the draft and wrote the manuscript. SG and CS revised the manuscript. All authors read and approved the final manuscript.

## FUNDING

## ACKNOWLEDGMENTS

Wohlfart, E., Wolff, J. O., Arzt, E., and Gorb, S. N. (2014). The Whole Is More Than the Sum of All its Parts: Collective Effect of Spider Attachment Organs. *J. Exp. Biol.* 217, 222–224. doi:10.1242/jeb.093468

Wolff, J. O., and Gorb, S. N. (2013). Radial Arrangement of Janus-like Setae Permits Friction Control in Spiders. *Sci. Rep.* 3, 1101. doi:10.1038/srep01101

Wolff, J. O., and Gorb, S. N. (2012c). Comparative Morphology of Pretarsal Scopulae in Eleven Spider Families. *Arthropod Struct. Dev.* 41, 419–433. doi:10.1016/j.asd.2012.04.004

Wolff, J. O., and Gorb, S. N. (2012a). Surface Roughness Effects on Attachment Ability of the Spider *Philodromus Dispar* (Araneae, Philodromidae). *J. Exp. Biol.* 215, 179–184. doi:10.1242/jeb.061507

Wolff, J. O., and Gorb, S. N. (2012b). The Influence of Humidity on the Attachment Ability of the Spider *Philodromus Dispar* (Araneae, Philodromidae). *Proc. R. Soc. B.* 279, 139–143. doi:10.1098/rspb.2011.0505

Xue, L., Steinhart, M., and Gorb, S. N. (2013). "Biological and Bioinspired Micro- and Nanostructured Adhesives," in *Biomaterials Surface Science, 409–439.* Editors A. Taubert, J. F. Mano, and J. C. Rodriguez-Cabello (Weinheim: Wiley VCH).

Xue, L., Kovalev, A., Thöle, F., Rengarajan, G. T., Steinhart, M., and Gorb, S. N. (2012). Tailoring normal Adhesion of Arrays of Thermoplastic, spring-like Polymer Nanorods by Shaping Nanorod Tips. *Langmuir* 28, 10781–10788. doi:10.1021/la3020354

Yang, X., Chen, L., Zhang, P., Zhong, H., Zhang, Y., Zhang, R., et al. (2020). Investigation of the Relationship between Adhesion Force and Mechanical Behavior of Vertically Aligned Carbon Nanotube Arrays. *Nanotechnol.* 31, 295701. doi:10.1088/1361-6528/ab85ed